Soft Matter

www.rsc.org/softmatter

Volume 8 | Number 1 | 7 January 2012 | Pages 1–236

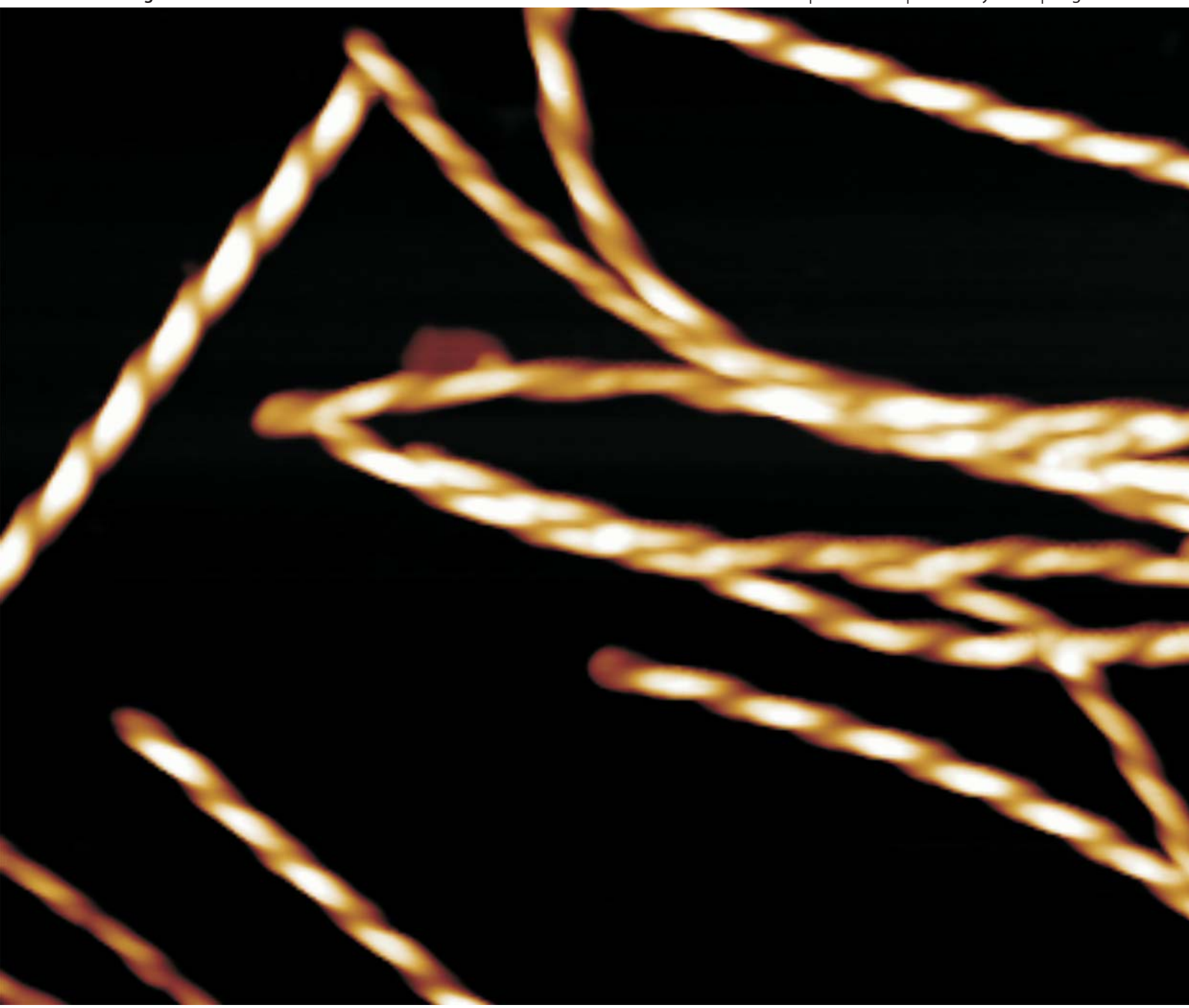

ISSN 1744-683X

RSC Publishing

PAPER

Antoni Sánchez-Ferrer *et al.*

Edible supramolecular chiral nanostructures by self-assembly of an amphiphilic phytosterol conjugate

1744-683X(2012)8:1;1-M

Soft Matter

Dynamic Article Links

Cite this: *Soft Matter*, 2012, **8**, 149

www.rsc.org/softmatter

PAPER

Edible supramolecular chiral nanostructures by self-assembly of an amphiphilic phytosterol conjugate†

Antoni Sánchez-Ferrer, Jozef Adamcik and Raffaele Mezzenga*

Received 15th August 2011, Accepted 30th September 2011
DOI: 10.1039/c1sm06560b

We study the self-assembly of a food-grade glucose-β-sitosterol conjugate in bulk and in solution by small angle X-ray scattering (SAXS) and atomic force microscopy (AFM). The amphiphilic behavior of the glucose-β-sitosterol conjugate, combined with the chirality of both its moieties, leads in solutions to the aggregation into supramolecular chiral aggregates with plate-like, spherical and helical ribbon configurations, depending on concentration and solvent quality. Owing to the crucial role of phytosterols in replacing cholesterol content and the need for functional edible fibrils with enhanced nutritional value, this system shows great promise in the struggle for the design of new functional food building blocks with targeted properties.

Introduction

Phytosterols are sterols extracted from plants, and have structures similar to that of cholesterol.[1–5] They are building blocks of biomembranes and precursors for hormones in plants.[6,7] They have been proposed as a natural source for the reduction of both cholesterol in blood plasma as well as cholesterol low-density lipoprotein, and recommended as a dietary supplement.[8–10] Besides regular phytosterols, conjugated phytosterols are also present in plants as fatty acids, acylated glycosides or glycoside derivatives.[1–3,6,7,11]

Phytosterols solubility is very low in water,[12] and their bioavailability is reduced when they are in the crystalline form.[13,14] A route to make them more soluble is to conjugate them to a polar group, such as sugars, which might enhance the solubility due to the presence of hydroxyl groups.[15] Alternatively, stable phytosterol colloidal particles have been obtained using non-ionic surfactants,[16,17] and different sizes (from 80 to 250 nm in diameter, and from 500 to 700 nm in length) or morphologies (rod-like and plate-like crystals)[18,19] have been observed.

Cholic acid ester derivatives with hydrophilic ethylene glycol tails[20] and other bile acid conjugates[21–24] have been reported to form gels. The former gels broke down to crystals with helical structures (pitch: 7.3 Å), with different dimensions depending on the handedness of the self-assembled structure (left-handed helical crystal: 1.6 μm diameter and 8.9 μm length; right-handed helical crystal: 4.8 μm diameter and 190 μm length). In hydrophobic media such as natural oils on the other hand, mixtures of γ-oryzanol with phytosterols associate in a synergistic way to form hollow tubular structures with diameter in the range of 6.7–8.0 nm and a wall thickness of 0.8–1.2 nm.[25–29]

Despite these encouraging works, the supramolecular self-aggregation behavior of these systems remains a complex, still poorly understood process, in which hydrophobic interactions, hydrogen bonding, crystallization, steric effects, and supramolecular chirality all concur to establish the final complex architectures.

In this work, we discuss for the first time the spontaneous self-assembly behaviour of a conjugated glucose–sitosterol (β-sitosterolin), synthesized in our laboratory, and an analogue of that found in almonds, cashews, sesame seeds, sunflower seeds, squash, barley, peas, olive oil, peanuts and cloves. We rely on small and wide angle X-ray scattering (SAXS, WAXS) and on atomic force microscopy (AFM). We discuss the complex architectures of the colloidal spheres, platelets and fibrils based on supramolecular β-sitosterolin self-assembly and we touch on the control of their morphologies by changing the solvent quality, concentration and aggregation time.

Experimental section

Materials

2,3,4,6-Tetra-*O*-acetyl-α-D-glucopyranosyl bromide (Fluka) and β-sitosterol (Sigma, ≥70%, with campesterol and β-sitostanol residual content) were used as received. Zinc bromide (Sigma-Aldrich) and the powdered 4A molecular sieves were dried at 120 °C for 24 h prior to use. CH_2Cl_2 was dried over CaH_2 and distilled before use. Dimethyl sulfoxide (DMSO), isopropanol (^{i}PrOH) and Milli-Q water were filtered through a PTFE syringe filter (0.2 μm) for the preparation of AFM and SAXS samples.

ETH Zurich, Food & Soft Materials Science, Institute of Food, Nutrition & Health, Schmelzbergstrasse 9, LFO, E23, 8092 Zürich, Switzerland. E-mail: raffaele.mezzenga@agrl.ethz.ch

† Electronic supplementary information (ESI) available: Detailed experimental procedures, sample preparation, SAXS, and AFM. See DOI: 10.1039/c1sm06560b

Apparatus and techniques

^{1}H NMR experiments were carried out at room temperature on a Bruker Avance Spectrometer operating at 400 MHz, and using $CDCl_3$ or DMSO-d_6 as solvents and as the internal standards.

Simultaneous small and wide-angle X-ray scattering (SAXS and WAXS, respectively) experiments were performed using a Rigaku MicroMax-002+ microfocused beam (4 kW, 45 kV, 0.88 mA) in order to obtain direct information on the SAXS and WAXS reflections. The Cu K_α radiation ($\lambda_{Cu\ K\alpha} = 1.5418$ Å) was collimated by three pinhole (0.4, 0.3, and 0.8 mm) collimators. The scattered X-ray intensity was detected by a Fuji Film BAS-MS 2025 imaging plate system (15.2 × 15.2 cm^2, 50 mm resolution) and a two-dimensional Triton-200 X-ray detector (20 cm diameter, 200 mm resolution), for WAXS and SAXS regions, respectively. An effective scattering vector range of 0.05 nm^{-1} < q < 25 nm^{-1} was obtained, where q is the scattering wave vector defined as $q = 4\pi\sin\theta/\lambda_{Cu\ K\alpha}$, with a scattering angle of 2θ.

Fourier-transform infrared (FTIR) spectra of solid samples were recorded at room temperature with a Varian 640 FTIR spectrometer and a MKII Golden Gate single attenuated total reflection (ATR) system.

ORD experiments were performed on an ORDM Jasco-815 polarimeter with a 5 cm length and 1 cm diameter cuvette in DMSO as solvent at 25 °C, and for the observation of the change in the optical rotation as function of the wavelength from 300 to 700 nm.

Tapping mode AFM was carried out on a Nanoscope 8 Multimode Scanning Force Microscope (Veeco). AFM cantilevers (Veeco, USA) for tapping mode in soft tapping conditions were used at a vibrating frequency of 150 kHz. Images were simply flattened using the Nanoscope 8.1 software, and no further image processing was carried out. A 30 μL aliquot of solution at a certain concentration of β-sitosterolin was deposited onto freshly cleaved mica or on highly ordered pyrolytic graphite (HOPG), incubated for 1 minute and dried in air.

Synthesis of β-sitosterolin tetraacetate (β-sitosteryl-2,3,4,6-tetra-*O*-acetyl-β-D-glucopyranoside)

In a 100 mL round-bottomed flask, 1.000 g (2.43 mmol) of 2,3,4,6-tetra-*O*-acetyl-α-D-glucopyranosyl bromide, 1.513 g (3.65 mmol) of β-sitosterol, 1.643 g (7.30 mmol) of zinc bromide, and 2.432 g of powdered 4A molecular sieves were placed, and after purging with nitrogen, 40 mL of anhydrous CH_2Cl_2 were added. The suspension was magnetically stirred and brought to reflux for 6 h under nitrogen atmosphere. The solution was filtered, washed several times with CH_2Cl_2 and evaporated. The residue was chromatographed in a silica gel column (EtAcO/cyclohexane (1 : 4)). Yield: 1.403 g (77%).

^{1}H NMR (400 MHz, $CDCl_3$): δ = 5.35 (1H, m, H6), 5.20 (1H, t, H3′, J = 9.5 Hz), 5.07 (1H, t, H4′, J = 9.6 Hz), 4.95 (1H, dd, H2′, J = 9.6 Hz, J = 8.1 Hz), 4.58 (1H, d, H1′, J = 10.4 Hz), 4.25 (1H, dd, H6′, J = 12.3 Hz, J = 4.7 Hz), 4.11 (1H, dd, H6′, J = 12.2 Hz, J = 2.5 Hz), 3.67 (1H, ddd, H5′, J = 9.9 Hz, J = 4.8 Hz, J = 2.4 Hz), 3.48 (1H, m, H3), 2.35 (1H, m, H4), 2.22 (1H, m, H4), 2.07 (3H, s, CH_3CO), 2.04 (3H, s, CH_3CO), 2.01 (3H, s, CH_3CO), 2.00 (3H, s, CH_3CO), 2.00–1.00 (27H), 0.98 (3H, s, H19), 0.91 (3H, d, H21, J = 6.0 Hz), 0.84 (3H, t, H29, J = 6.3 Hz), 0.82 (3H, d, H27, J = 6.1 Hz), 0.79 (3H, d, H26, J = 6.3 Hz), 0.67 (3H, s, H18) ppm (see ESI, Chart S1†).

Synthesis of β-sitosterolin (β-sitosteryl-β-D-glucopyranoside)

In a 250 mL round-bottomed flask with magnetic stirring, 1.000 g (1.34 mmol) of β-sitosteryl-2,3,4,6-tetra-*O*-acetyl-β-D-glucopyranoside was dissolved in 100 mL of a mixture of 0.25 M NaOH/THF/MeOH (1 : 2 : 1). The system was magnetically stirred at room temperature and the hydrolysis was kept for 4 h. The white solid that appeared was filtered out, washed several times with a cold mixture of THF/H_2O, and dried under vacuum. Yield: 0.504 g (36%).

^{1}H NMR (400 MHz, DMSO-d_6): δ = 5.33 (1H, m, H6), 4.87 (3H, s, OH), 4.42 (1H, s, OH), 4.22 (1H, d, H1′, J = 7.6 Hz), 3.63 (1H, dd, H3′, J = 10.8 Hz, J = 4.3 Hz), 3.43 (1H, m, H3), 3.18–2.96 (4H, m, H2′-H5′-2H6′), 2.89 (1H, t, H4′, J = 8.2 Hz), 2.35 (1H, m, H4), 2.12 (1H, m, H4), 2.00–1.00 (27H), 0.96 (3H, s, H19), 0.90 (3H, d, H21, J = 6.4 Hz), 0.89 (3H, t, H29, J = 6.0 Hz), 0.82 (3H, d, H27, J = 6.1 Hz), 0.80 (3H, d, H26, J = 5.9 Hz), 0.65 (3H, s, H18) ppm (see ESI, Chart S2†).

Preparation of the self-assembled samples

AFM and SAXS samples were prepared from DMSO solutions of β-sitosterolin. From an initial concentration of β-sitosterolin in DMSO, the sample was diluted 10 times by adding drop wise water or isopropanol. AFM samples had a concentration ranging from 0.1 to 0.01 w/w% of β-sitosterolin. SAXS samples had a concentration ranging from 1 to 0.1 w/w%. For the SWAXS powder diffraction experiment, β-sitosterolin was prepared by drying under vacuum the sample that appeared after the final synthetic step.

Results and discussion

Synthesis and characterization of β-sitosterolin

The β-sitosterol conjugate was synthesized in two steps (Scheme 1). The first reaction was the nucleophilic substitution in which a tetraacetyl protected α-D-glucose containing bromide as a living group in the anomeric carbon reacted with the hydroxyl group from the β-sitosterol in the presence of a Lewis acid in anhydrous media.[30] The final amphiphilic molecule β-sitosterolin was obtained *via* hydrolysis in basic conditions of the four acetyl protecting groups in the sugar moiety.[31] The chemical structures of both molecules (β-sitosterolin tetraacetate and β-sitosterolin) were confirmed by their corresponding ^{1}H NMR spectra,[32–34] solubility tests, Fourier-transform infrared spectroscopy (FTIR) and optical rotatory dispersion (ORD) experiments.

D-Glucose ($\delta_{D\text{-glucose}} = 37.8$ MPa$^{1/2}$, log $P_{D\text{-glucose}} = -1.88$)[35] is soluble in DMSO ($\delta_{DMSO} = 26.7$ MPa$^{1/2}$, log $P_{DMSO} = -1.35$)[36,37] and water ($\delta_{water} = 47.8$ MPa$^{1/2}$),[36,37] but insoluble in ^{i}PrOH ($\delta_{iso\text{-}PrOH} = 23.5$ MPa$^{1/2}$, log $P_{iso\text{-}PrOH} = 0.16$).[36,37] β-Sitosterol ($\delta_{\beta\text{-sitosterol}} = 18.4$ MPa$^{1/2}$, log $P_{\beta\text{-sitosterol}} = 10.73$)[38] is soluble in DMSO and ^{i}PrOH, but not in water. The amphiphilic molecule β-sitosterolin ($\delta_{\beta\text{-sitosterolin}} = 28.1$ MPa$^{1/2}$, log $P_{\beta\text{-sitosterolin}} = 8.78$) is soluble only in DMSO, and when adding water or ^{i}PrOH a precipitate, which remains stable as a suspension, is formed. Thus, DMSO is a good solvent for both moieties

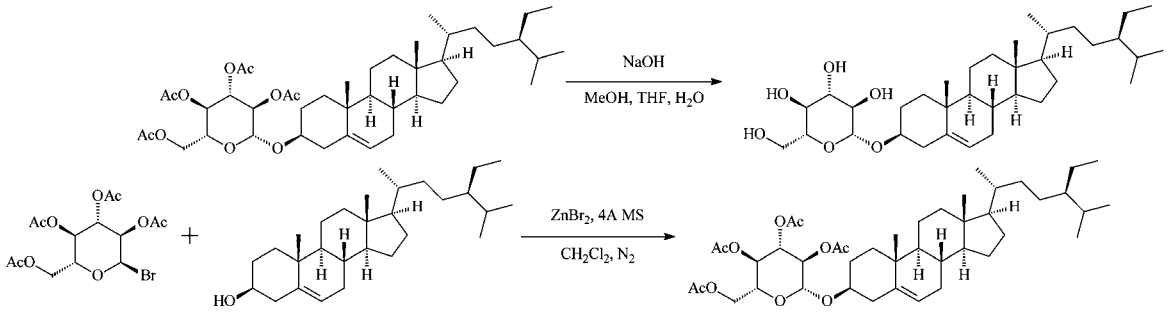

Scheme 1 Synthetic route followed to produce β-sitosterolin.

in β-sitosterolin, and water and ^{i}PrOH are only selective solvents for one of the building blocks. As it will be shown below, this enables for the control of the self-aggregating behaviour of β-sitosterolin by dispersing its DMSO molecular solution into either of the two selective solvents.

ORD experiments show the optical activity of the conjugated molecule in DMSO, when the molecule is fully soluble. D-Glucose is a dextrorotatory molecule with a specific rotation of $[\alpha]_D = +57.3°$ measured at 25 °C in DMSO, while both β-sitosterol and β-sitosterolin are levorotatory molecules with specific rotations of $[\alpha]_D = -18.6°$ and $[\alpha]_D = -10.0°$, respectively (Fig. 1a). The low value of the specific rotation of β-sitosterolin[39] is due to the presence of co-existing β-sitostanolin, which is a dextrorotatory molecule and averages the final optical rotatory power of the phytosterol conjugate.

ATR-FTIR experiments of β-sitosterolin showed the presence of characteristic vibrational modes from both D-glucose (st OH, st, C–OH, and st C–O–C) and β-sitosterol (st C–H, st and δ C=C, and δ from CH_3 and CH_2) (Fig. 1b).

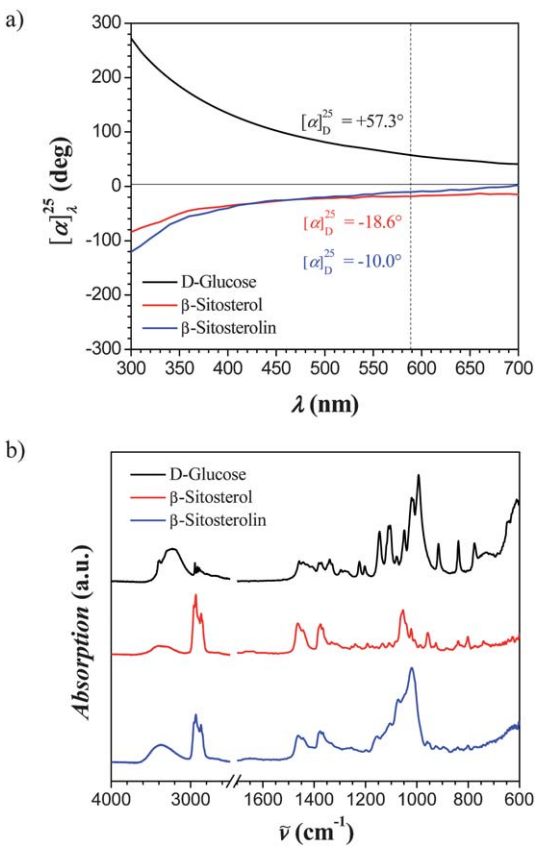

Fig. 1 (a) Optical rotatory dispersion (ORD) spectra of D-glucose, β-sitosterol and β-sitosterolin as function of the transmitted wavelength. (b) ATR-FTIR spectra of D-glucose, β-sitosterol and β-sitosterolin showing the presence of characteristic vibrational modes from both D-glucose and β-sitosterol.

Self-assembly of β-sitosterolin

In order to understand the driving force to form supramolecular aggregates in a selective solvent, we first studied the self-assembly behaviour in bulk, where the head–tail interactions of β-sitosterolin are not mediated by either ^{i}PrOH or water. A very strong micro-phase separation between the polar glucose head group and the apolar rigid sitosteryl tail is found, as revealed by the Small and Wide Angle X-ray Scattering (SWAXS) diffractogram of the dry powder sample shown in Fig. 2 after drying the synthesized sample under vacuum.

The eleven Bragg diffraction peaks with a spacing of $d = 4.5$ nm and a correlation length of $\xi = 49.3$ nm indicate a perfectly ordered lamellar phase, in which the β-sitosterolin molecules form bilayered domains composed of two facing glucose heads and two sitosteryl skeletons (Fig. 2), and witness the very high incompatibility between the polar head and hydrophobic tail of β-sitosterolin.

When adding drop-wise water or ^{i}PrOH (poor solvents) into a DMSO (good solvent) solution of β-sitosterolin, cloudy dispersions were rapidly obtained (see ESI, Fig. S1†). The SAXS pattern of these dispersions showed the presence of different types of aggregates (Fig. 3). β-Sitosterolin was also dispersed in pure ^{i}PrOH which was stable upon time, while once dispersed in pure water it precipitated. This is the basis for understanding the relatively flat signal of 1 wt% β-sitosterolin in H_2O shown in Fig. 3a, as opposed to all other scattering profiles.

All samples prepared by addition of ^{i}PrOH or water in DMSO show a scattering peak at around $q = 1.40$ nm^{-1} (arrows in Fig. 3) which corresponds to the micro-phase separation length scale 4.5 nm already observed in the solid state. Thus, micro-phase separation at this small length scale is maintained also in solution, irrespective of the selective solvent considered. However, this peak was considerably sharper in the case of water as solvent.

From the shape of the peak at $q = 1.40$ nm^{-1}, the correlation length ξ was evaluated and by diluting the sample a decrease in its value was observed. Samples in ^{i}PrOH/DMSO (9 : 1)

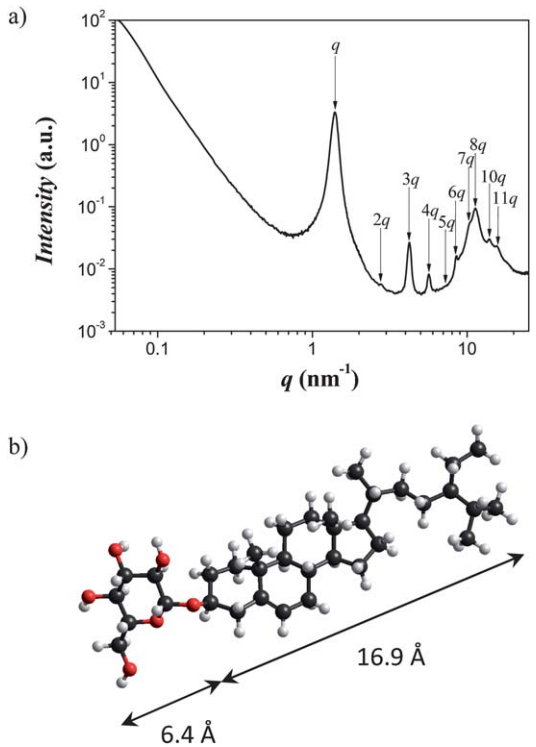

Fig. 2 (a) SWAXS profile pattern for β-sitosterolin in the solid state indicating self-assembly into a lamellar phase of period 4.5 nm. (b) The chemical structure and dimensions of the polar head and apolar tail group, match precisely the half-period of the lamellar phase.

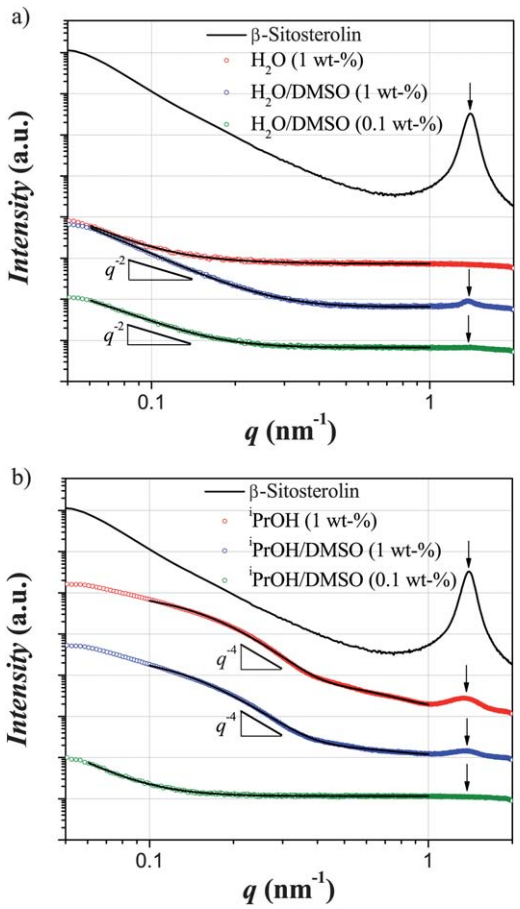

Fig. 3 SAXS pattern for dispersions of (a) 1 w/w% β-sitosterolin in pure H_2O, 1 w/w% in H_2O/DMSO (9 : 1), 0.1 w/w% in H_2O/DMSO (9 : 1), and (b) 1 w/w% β-sitosterolin in pure ^{i}PrOH, 1 w/w% in ^{i}PrOH/DMSO (9 : 1), 0.1 w/w% in ^{i}PrOH/DMSO (9 : 1) together with their corresponding fitting curves. *Note*: the continuous top black curve is the scattering pattern of solid β-sitosterolin.

(Fig. 3b) showed correlation lengths from 16.4 to 3.6 nm at 1 and 0.1 w/w% concentrations, respectively. For samples in H_2O/DMSO (9 : 1), values from 35.1 to 8.2 nm were found at the same respective concentrations, indicating that water promotes more strongly correlated structures compared to ^{i}PrOH, probably due to the high insolubility (stronger aggregation) of the β-sitosterolin molecule in water (see ESI, Fig. S2†).

Another key point is the shape of scattering curves in the low q limit (0.06–1.0 nm^{-1}). In water, a q^{-2} power-law decrease is observed, indicative of platelet-like sharp interfaces, while in ^{i}PrOH, samples show a bump with a slope value from 3.5 to 3.8, indicative of polydisperse sphere-like structures, with average radius from 20 to 30 nm. This is an indication of different morphological structures in the aggregates at larger length scales ranging from 6 to 100 nm (see ESI, Fig. S3†).

A first rationale into the shape of the expected morphologies in either water or ^{i}PrOH can be obtained by considering the mismatch in volume fraction of the polar head group ($\phi_{Glucose}$ = 0.20) and the rigid apolar tail ($\phi_{Sitosterol}$ = 0.80): when ^{i}PrOH is present, β-sitosterol will be exposed against the solvent and $\phi_{Sitosterol}/\phi_{Glucose} = 4.1$ is high enough to enable the formation of spherical-like micelles. On the other hand, when water makes up the majority of the solvent, glucose will be exposed against water, and the ratio $\phi_{Glucose}/\phi_{Sitosterol} = 0.25$ is so low that spherical micelles are no longer expected and aggregates with a more flat-like interface will be promoted. The fact that the $q = 1.40$ nm^{-1} reflection is maintained both in the solid state and in solvent dispersions, that is to say that no swelling of the bilayer spacing is observed, further suggests that solvation effects should not greatly affect the $\phi_{Glucose}/\phi_{Sitosterol}$ and the reasoning given above.

Further insight into the structures of the aggregates was gained by AFM. At high concentrations (1 w/w%), samples in H_2O/DMSO (9 : 1) were confirmed to adopt a flat-like structure—glucose occupying the outer part of the flat side (see ESI, Fig. S4†)—in which the thickness is clearly defined by multilayers of steps of 4.7 nm (Fig. 4a), so that the total width of these flat-like structures is an integer multiple of 4.7 nm. At lower concentrations (0.1 w/w%), some flat-like objects break down into highly elongated ribbons wrapping into helical ribbons of typical diameter of 24 ± 5 nm and pitch of 90 ± 10 nm. Fig. 4b gives a typical AFM image for these helical ribbons, while the height profile allows unambiguous identification of the topology of the ribbon as helical. The transition from flat-like structure to helical ribbons can be explained by the diminishing probability to form large plates when decreasing the concentration. Indeed, helical ribbons are known to undergo structural transitions associated with their width.[40] The real width of the ribbon W was estimated using the equation $W = S\sin\gamma$, where γ is the tilt angle of the helical ribbon edges with respect to the fibril axis (Fig. 4b).

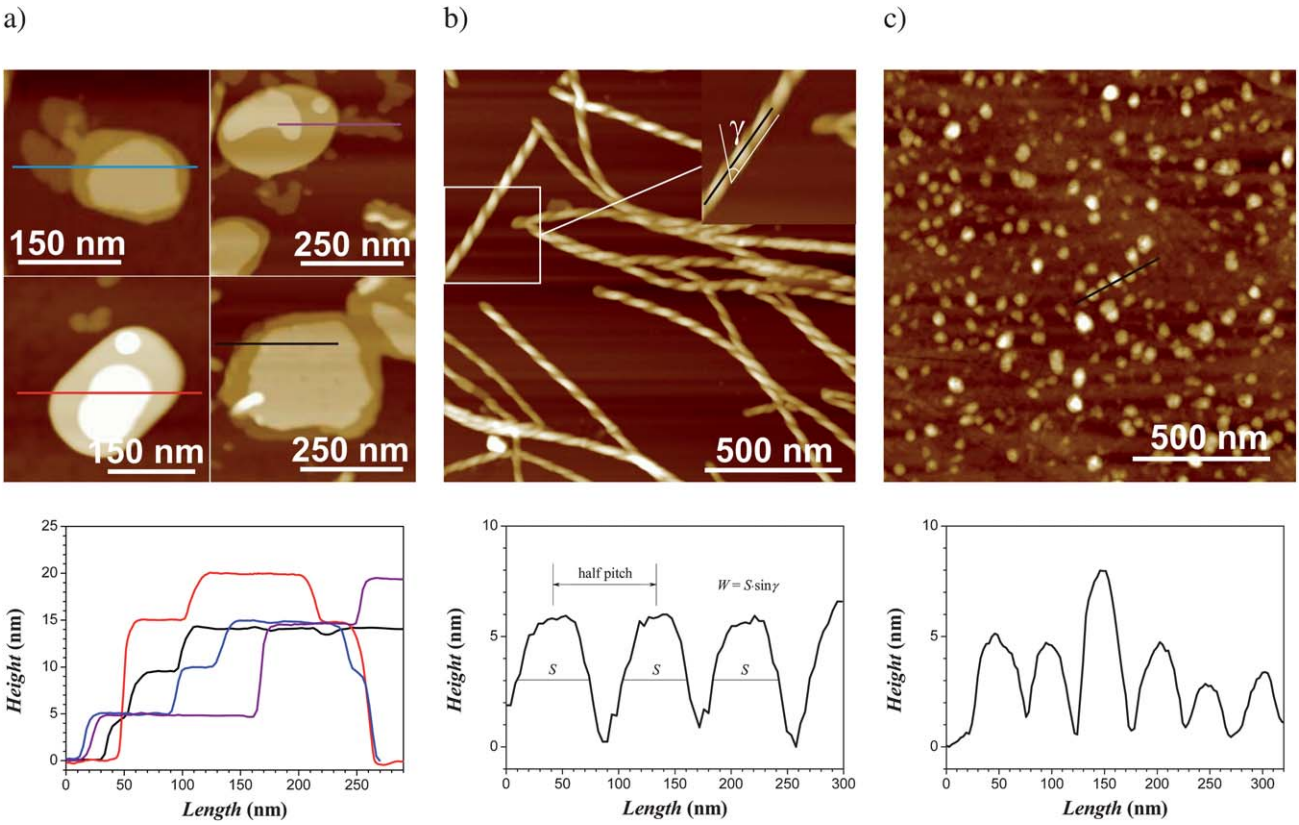

Fig. 4 AFM height images of the self-assembly of 0.1 w/w% β-sitosterolin in H_2O/DMSO (9 : 1) showing (a) platelet-like structures and their height profile with quantized thickness and (b) coexisting helical ribbons with the corresponding analysis of the height profile and the pitch. AFM height images of the self-assembly of 0.1 w/w% β-sitosterolin in ^{i}PrOH/DMSO (9 : 1) showing (c) spherical aggregates and their height profile. From (a) to (c), the lower row gives the height profile measured along the colored lines of the corresponding upper AFM images.

By measuring the average width of helical ribbons $S = 60 \pm 10$ nm in the full-width half-maxima of the cross-section and measuring a tilt angle of $\gamma = 40° \pm 5°$, one easily finds a typical width of 39 ± 5 nm for helical ribbons. These ribbons can then coil up due to the chirality of the rigid sitosterol skeleton molecule, while maintaining the sugar moieties exposed against the water-rich solvent. We stress here that due to the low volume fraction of helical ribbons *vs.* platelets and the consistency of the large width of the ribbons with the q^{-2} slope measured at $q < 0.2$ nm^{-1}, SAXS analysis alone would not allow resolution of these helical ribbons. The handedness of the ribbons, identified as left as in the case of the sitosterol unit, demonstrates that supramolecular chirality assists the coiling of the ribbons. Previous circular polarized light experiments showed a selective reflection at certain frequency for which the left polarized light matched the same handedness as the steroidal medium.[41,42]

Samples in ^{i}PrOH showed rarely the population of plate-like structures (sitosterol exposed against the solvent in the outer part of the plates) of steps of 4.7 nm, similar to water, and the dominant population was that of objects of 4 to 5 nm in height and 40–50 nm in diameter (Fig. 4c), but without quantized heights. This immediately indicates that these aggregates are larger than single β-sitosterolin micelles. The SAXS analysis shown in Fig. 3b suggests spherical aggregates of 20–30 nm radius, with an internal feature size corresponding to $2\pi/q$, with $q = 1.4$ nm^{-1} (*e.g.* 4.5 nm); while the diameter observed by AFM is in the range of features extracted from the SAXS analysis, the lower height observed by AFM for these objects, which is consistent with a bilayer or a single micelle, could result from the spreading of a multi-micellar aggregate into the surface of the substrate upon adsorption. As already discussed, the high ratio in the sitosterol/glucose volume fraction does not promote in the present case the formation of self-organized aggregates with large lateral feature size, stabilizing spherical-like aggregates with smaller size.

The formation of the supramolecular colloidal aggregates reported here is caused by the sudden change in the solvent quality (polarity, hydrogen bonding, apolar interactions) of the solution. Addition of a co-solvent[43–47] which is miscible with the good initial organic solvent but which is selective for specific moieties of β-sitosterolin induces the self-assembly of this molecule into supramolecular aggregates as schematically summarized in Fig. 5. The final, self-assembled structures observed here bear several similarities with the topologies of other supramolecular aggregates based on model peptides[40,48] and surfactants[49,50] inferring the generality of the self-assembly mechanisms involved. Although several research reports have been published for colloidal particles formed from chiral molecules,[51–59] the relation between molecular chirality and supramolecular chirality is not conclusively solved yet, and the present findings can provide additional elements to the process of unravelling this complex and fascinating problem.

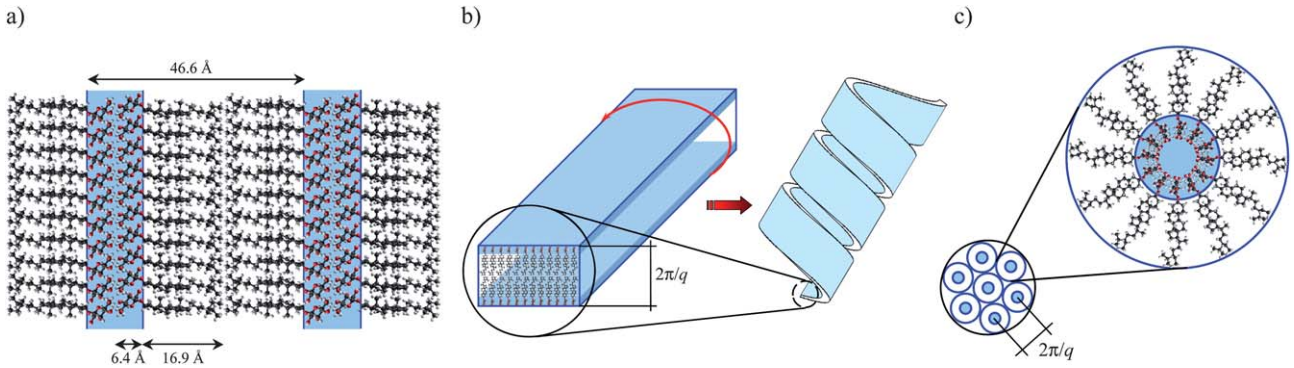

Fig. 5 Self-assembly of β-sitosterolin: (a) bilayer aggregation, (b) lamination and helical winding of the bilayer aggregates in the presence of water, and (c) spherical aggregation in the presence of isopropanol.

Conclusions

The self-assembly of a phytosterol conjugate (β-sitosterolin) has been investigated in bulk, in molecular solution and in the presence of a selective solvent. Depending on the quality of the selective solvent, the molecule aggregates into molecular bilayers, in which the moieties facing the solvent can be either the glucose or sitosterol units, depending on whether water or isopropanol is used as solvent, respectively.

In the first case (water), platelet-like structures with thickness equal to an integer multiple of the bilayer period (4.7 nm) are formed, which upon dilution transform into left-handed helical ribbons, whose supramolecular chirality is induced by packing of the sitosterol moieties. In the second case (isopropanol), spherical-like objects much smaller in size are formed, as a consequence of the high volume fraction of the sitosterol moieties as opposed to that of glucose.

These findings may both contribute to the understanding of supramolecular chirality in the self-aggregation process of chiral molecules, as well as to provide an appealing new system for the design of edible fibrils with desirable nutritional components.

Acknowledgements

The authors acknowledge Prof. Laura Nyström (ETH Zurich) for valuable and inspiring discussions.

References

1 L. J. Goad, *Methods Plant Biochem.*, 1991, **7**, 369–434.
2 L. J. Goad and T. Akihisa, *Analysis of Sterols*, Blackie, London, 1997.
3 N. V. Kovganko and Z. N. Kashkan, *Chem. Nat. Compd.*, 1999, **35**, 479–497.
4 R. E. Ostlund, *Curr. Opin. Lipidol.*, 2004, **15**, 37–41.
5 R. E. Ostlund, *Lipids*, 2007, **42**, 41–45.
6 A. Tietz, *Z. Naturforsch., C: J. Biosci.*, 1981, **36**, 900–901.
7 M. A. Hartmann and P. Benveniste, *Methods Enzymol.*, 1987, **148**, 632–650.
8 A. Ambring, P. Friberg, M. Axelsen, M. Laffrezen, M. R. Taskinen, S. Basu and M. Johansson, *Clin. Sci.*, 2004, **106**, 519–525.
9 S. M. Mel'nikov, J. W. M. S. ten Hoorn and A. P. A. M. Eijkelenboom, *Chem. Phys. Lipids*, 2004, **127**, 121–141.
10 L. Calpe-Berdiel, J. C. Escolà-Gil and F. Blanco-Vaca, *Atherosclerosis*, 2009, **203**, 18–31.
11 M. Ohnishi and Y. Fujino, *Phytochemistry*, 1981, **20**, 1357–1358.
12 G. Brufau, M. A. Canela and M. Rafecas, *Nutr. Res.*, 2008, **28**, 217–225.
13 O. J. Pollak, *Circulation*, 1953, **7**, 702–706.
14 V. Piironen, D. G. Lindsay, T. A. Miettinen, J. Toivo and A. M. Lampi, *J. Sci. Food Agric.*, 2000, **80**, 939–966.
15 P. Breinhölder, L. Mosca and W. Lindner, *J. Chromatogr., B: Anal. Technol. Biomed. Life Sci.*, 2002, **777**, 67–82.
16 L. Rossi, J. W. M. Seijen ten Hoorn, S. M. Melnikov and K. P. Velikov, *Soft Matter*, 2010, **6**, 928–936.
17 L. Rossi, S. Sacanna and K. P. Velikov, *Soft Matter*, 2011, **7**, 64–67.
18 L. I. Christiansen, J. T. Rantanen, A. K. von Bonsdorff, M. A. Karjalainen and J. K. Yliruusi, *Eur. J. Pharm. Sci.*, 2002, **15**, 261–269.
19 H. Kawachi, R. Tanaka, M. Hirano, K. Igarashi and H. Ooshima, *J. Chem. Eng. Jpn.*, 2006, **39**, 869–875.
20 X. Wang, Y. Lu, Y. Duan, L. Meng and C. Li, *Adv. Mater.*, 2008, **20**, 462–465.
21 S. Mukhopadhyay and U. Maitra, *Curr. Sci.*, 2004, **87**, 1666–1683.
22 P. Babu, N. M. Sangeetha and U. Maitra, *Macromol. Symp.*, 2006, **241**, 60–67.
23 S. Banerjee, R. K. Das and U. Maitra, *J. Mater. Chem.*, 2009, **19**, 6649–6687.
24 P. Terech, S. Dourdain, S. Bhat and U. Maitra, *J. Phys. Chem. B*, 2009, **113**, 8252–8267.
25 M. Pernetti, K. F. van Malssen, E. Flöter and A. Bot, *Curr. Opin. Colloid Interface Sci.*, 2007, **12**, 221–231.
26 A. Bot, R. den Adel and E. C. Roijers, *J. Am. Oil Chem. Soc.*, 2008, **85**, 1127–1134.
27 A. Bot, Y. S. J. Veldhuizen, R. den Adel and E. C. Roijers, *Food Hydrocolloids*, 2009, **23**, 1184–1189.
28 A. Bot, R. den Adel, E. C. Roijers and C. Regkos, *Food Biophys.*, 2009, **4**, 266–272.
29 M. A. Rogers, *Food Res. Int.*, 2009, **42**, 747–753.
30 T. Murakami, Y. Sato and M. Shibakami, *Carbohydr. Res.*, 2008, **343**, 1297–1308.
31 C. Gauthier, J. Legault, M. Lebrun, P. Dufour and A. Pichette, *Bioorg. Med. Chem.*, 2006, **14**, 6713–6725.
32 J. Seki, A. Okita, M. Watanabe, T. Nakagawa and K. Honda, *J. Pharm. Sci.*, 1985, **74**, 1259–1264.
33 E. Isik, T. Sabudak and S. Oksuz, *Chem. Nat. Compd.*, 2007, **43**, 614–615.
34 O. Akpinar and M. H. Penner, *J. Carbohydr. Chem.*, 2008, **27**, 188–199.
35 K. L. Hoy, *J. Paint Technol.*, 1970, **42**, 115–118.
36 C. M. Hansen, *J. Paint Technol.*, 1967, **39**, 505.
37 A. F. M. Barton, *Handbook of Solubility Parameters and Other Cohesion Parameters*, CRC Press, Inc., Boca Raton, Florida, 1983.
38 A. Martin, P. L. Wu, Z. Liron and D. S. Cohen, *J. Pharm. Sci.*, 1985, **74**, 638–642.
39 A. S. R. Anjaneyulu and S. N. Raju, *Phytochemistry*, 1987, **26**, 2805–2810.
40 J. Adamcik, V. Castelletto, S. Bolisetty, I. W. Hamley and R. Mezzenga, *Angew. Chem., Int. Ed.*, 2011, **50**, 5495–5498.
41 J. Schmidtke, W. Stille, H. Finkelmann and S. T. Kim, *Adv. Mater.*, 2002, **14**, 746–749.
42 J. Schmidtke, S. Kniesel and H. Finkelmann, *Macromolecules*, 2005, **38**, 1357–1363.

43 L. Mukhopadhyay, P. K. Bhattacharyya, A. R. Das and S. P. Moulik, *Colloid Polym. Sci.*, 1993, **271**, 793–798.
44 D. Horn and J. Rieger, *Angew. Chem., Int. Ed.*, 2001, **40**, 4330–4361.
45 F. Q. Hu, S. P. Jiang, Y. Z. Du, H. Yuan, Y. Q. Ye and S. Zeng, *Colloids Surf., B*, 2005, **45**, 167–173.
46 M. E. Matteucci, M. A. Hotze, K. P. Johnston and R. O. Williams, *Langmuir*, 2006, **22**, 8951–8959.
47 V. Uskokovic and E. Matijevic, *J. Colloid Interface Sci.*, 2007, **315**, 500–511.
48 E. T. Pashuck, H. Cui and S. I. Stupp, *J. Am. Chem. Soc.*, 2010, **132**, 6041–6046.
49 R. Oda, I. Huc, M. Schmutz, S. J. Candau and F. C. MacKintosh, *Nature*, 1999, **399**, 566–569.
50 L. Ziserman, H. Y. Lee, S. R. Raghavan, A. Mor and D. Danino, *J. Am. Chem. Soc.*, 2011, **133**, 2511–2517.
51 J. H. Fuhrhop, P. Schnieder, E. Boekema and W. Helfrich, *J. Am. Chem. Soc.*, 1988, **110**, 2861–2867.
52 D. S. Chung, G. B. Benedek, F. M. Konikoff and J. M. Donovan, *Proc. Natl. Acad. Sci. U. S. A.*, 1993, **90**, 11341–11345.
53 R. J. H. Hafkamp, B. P. A. Kokke, I. M. Danke, H. P. M. Geurts, A. E. Rowan, M. C. Feiters and R. J. M. Nolte, *Chem. Commun.*, 1997, 545–546.
54 Y. V. Zastavker, N. Asherie, A. Lomakin, J. Pande, J. M. Donovan, J. M. Schnur and G. B. Benedek, *Proc. Natl. Acad. Sci. U. S. A.*, 1999, **96**, 7883–7887.
55 E. Grelet and S. Fraden, *Phys. Rev. Lett.*, 2003, **90**, 198302.
56 E. Barry, Z. Hensel, Z. Dogic, M. Shribak and R. Oldenbourg, *Phys. Rev. Lett.*, 2006, **96**, 018305.
57 Z. Dogic and S. Fraden, *Curr. Opin. Colloid Interface Sci.*, 2006, **11**, 47–55.
58 F. Tombolato, A. Ferrarini and E. Grelet, *Phys. Rev. Lett.*, 2006, **96**, 258302.
59 K. L. Kohlstedt, F. J. Solis, G. Vernizzi and M. O. de la Cruz, *Phys. Rev. Lett.*, 2007, **99**, 030602.